The Use of Proton Affinity Distributions for the Characterization of Active Sites of Alumina-Supported Co–Mo Catalysts

Michiaki Adachi,[1] Cristian Contescu,[2] and James A. Schwarz[3]

Department of Chemical Engineering and Materials Science, Syracuse University, Syracuse, New York 13244-1190

A series of MoO$_3$/Al$_2$O$_3$ catalysts of varying weight loading were characterized after calcination by their buffering capacity during potentiometric titration. Strong buffering of the aqueous electrolyte occurred in distinct pH ranges, which indicated the formation of hydrolysis products of the surface compounds formed in these pH windows. Addition of cobalt, followed by calcination, revealed a new feature which signaled the formation of a possible surface heteropolymolybdate compound. If cobalt was added first this compound was not formed, however, if cobalt and molybdenum were coimpregnated it was detectable. As a promoter, Ni(II) had an effect similar to cobalt, but Fe(III) did not.

The series of catalysts were further tested for their hydrodesulfurization activity using thiophene as a reactant. The thiophene conversion, as a function of the amount of surface compound formed by addition of the cobalt promoter, resulted in a linear relation, indicating that the Co/Mo compound detected in the oxidic state could be correlated with the HDS activity of these catalysts. © 1996 Academic Press, Inc.

INTRODUCTION

On alumina supports, tungsten or molybdenum in combination with nickel and/or cobalt have been the traditional catalysts used for hydrotreating feedstocks. Their importance in environmental catalysis is to produce cleaner fuels by significant removal of heteroatoms and aromatic compounds. Despite the critical importance and extensive use of these materials in commercial processes, the physical-chemical architecture of the active sites on these catalysts has yet to be determined unequivocally.

Most fundamental studies designed to elucidate the nature of the active sites have been directed at the catalyst in its sulfided state. Topsøe and co-workers (1, 2) proposed

on the basis of Mössbauer Emission Spectroscopy (MES) a ''Co–Mo–S'' model for the active site, while Louwers and Prins proposed, on the basis of extended X-ray absorption fine structure (EXAFS), the presence of a square pyramidal structure when Ni–Mo catalysts were sulfided (3). In model electron microscopy studies by Upton and co-workers it was demonstrated that Mo disulfide interacted with group eight metals (4). Kabe and co-workers used the concept of an Ni–Mo–S interaction species to support their results that it was an active site for hydrodesulfurization of dibenzothiophene in their study using a radio-isotope ^{35}S tracer technique (5). But these earlier and very recent reports are not totally unambiguous. For example, Crajé and co-workers have proposed, based on MES, that Mo in sulfided Co–Mo can be considered as a secondary support to increase the dispersion of the ''Co-sulfide'' species (6–8).

If Co interacts strongly with Mo in the sulfided catalysts, then it would seem logical to pursue the hypothesis that it also interacts strongly in the oxidic precursor state. With this as a basis Topsøe found a difference in the IR spectra of adsorbed NO on Co/Mo/Al$_2$O$_3$ compared to Co/Al$_2$O$_3$ catalysts (9). Additional evidence supporting the presence of interaction species on the oxidic state of Ni and Co/Mo catalysts was reported by Kasztelan and co-workers on the basis of their ion scattering spectroscopy (ISS) results (10). MES (11) and EXAFS (12, 13) were used to characterize hydrotreating catalysts in the oxide state and results led to the conclusion that there is a relationship between the amount of 6-coordinated Co and HDS activity. However, a later study by van Veen *et al.* (14) showed that a substantial fraction of the tetrahedral Co is also found to be capable of entering ''Co–Mo–S'' upon sulfidation. Laser Raman spectroscopy (LRS) (15, 16), and X-ray photoelectron spectroscopy (XPS) (16) have been also used to characterize the oxide surface.

Recently, using temperature-programmed reduction and XPS as techniques, work from our laboratory showed that Co–W interaction species were present on Co/WO$_3$/Al$_2$O$_3$ catalysts and that they appeared to exhibit a higher

---

[1] Permanent address: Central Technical Research Laboratory, Nippon Oil Co., Ltd., 8 Chidori-cho, Naka-ku, Yokohama, 231 Japan.
[2] Permanent address: Institute of Physical Chemistry of Romanian Academy, Spl. Independentei 202, Bucharest 77208, Romania.
[3] To whom correspondence should be addressed.

turnover frequency for methane formation than either Co or WO_3 on Al_2O_3 alone (17). We extended this work to examine the effect of different catalyst preparation protocols on the formation of Ni–W interaction species (18). Here it was found that catalysts formed by the incipient wetness procedure and adsorption impregnation and either dried, calcined, or reduced during pretreatment contained a persistent Ni–W interaction species despite the number of temperature-programmed reduction/temperature-programmed oxidation cycles to temperatures over 1300 K. It was apparent from these results that a unique template formed during the preparation steps, which was characteristic of a structure in which a strong metal–metal interaction was present.

The basis for the present study had its roots in the earlier work from our laboratory cited above and was conditioned by our recent developments to access the influence of additives to oxide supports, as well as the supports themselves, from their potentiometric titration in aqueous electrolytes (19). The literature on this subject is developing and the reader is referred to an appropriate reference (20). We will limit our discussion only to the practical application of these procedures to the catalysts studied here.

Potentiometric titration laboratory data can be directly converted to proton adsorpton isotherms (19). If a sufficient number of data points are collected, an isotherm can be constructed and it was shown that by proper analytical fitting and if an objective criterion for smoothing is applied, the affinity spectrum (19) of the substrate for protons can be determined. Two levels of analysis have been applied: the first deals with those systems in which the kernel of the integral equation, i.e., the proton isotherm, is described by a Langmuir isotherm, and the second with the case when the proton binding/release is due to hydrolysis of surface compounds on the oxide support (21). The former case has been documented in a recent report (22); the latter case applies here.

Transition metals oxides (TMO), such as Mo and W on Al_2O_3, have been studied extensively by a variety of techniques and in particular by Wachs and co-workers, using LRS (23). Recently, they reported on the effect of exposure of the support to ambient conditions, concluding that the second-phase oxide's structure reverted to that which would be present in the aqueous phase of the salt of the oxide precursor at a pH value corresponding to the pzc of the supported TMO (23). Our potentiometric titration of a series of WO_3/Al_2O_3 supports confirmed their finding and provided additional information on the surface chemistry of these TMOs as starting materials for addition of other elements. Thus the interaction of Co with a Mo oxide/Al_2O_3 support requires some knowledge of the state of Mo oxide on Al_2O_3 during the impregnation process.

When Mo supported on Al_2O_3 is subjected to potentiometric titration, the second-phase oxide undergoes hydrolysis reactions which is signaled by significant changes in the charging behavior of the support as a function of pH. The affinity distribution provides a signature which is dependent on the Mo loading. If another element is added, such as Co, and it interacts strongly with Mo, then we might expect some change in the affinity spectrum due to changes in the structures undergoing the hydrolysis reactions. Furthermore, if Co oxide alone does not alter the affinity spectrum of Al_2O_3, then new features in the affinity spectra for Co–Mo–Al_2O_3 catalysts in their oxidic state might be correlated with the performance of these materials in a HDS test reaction. Indeed, this is what we found.

Although other techniques have been used to study these oxidic precursors to HDS working catalysts, they are generally expensive, time-consuming, and require special handling of the specimen. Potentiometric titration data can be obtained quickly with equipment that is commonly available in most analytical laboratories. This approach provides a powerful method for characterization of catalysts and its surface sensitivity is unambiguous, which contrasts with other techniques. Recently we have shown that a relationship could be established between the proton affinity of several mixed oxides in an aqueous environment and their catalytic activity for 1-butene isomerization (22). In the present paper, we focus on the relationship between the buffering capacity changes that result as a consequence of TMOs as revealed in proton affinity distributions (PADs) of Co–Mo/Al_2O_3 catalysts in the oxidic phase and their performance as HDS catalysts after sulfidation. The catalysts described in this paper have been subjected to additional characterization by XPS, Raman, and TPR to provide corroborating evidence for confirming the conclusion of the present paper. Those results will be presented in a subsequent paper. The methodology described herein provides a basis for predicting the performance of the sulfided catalyst before presulfiding and activity tests are conducted, steps which can add significantly to process costs in commercial size applications.

EXPERIMENTAL

Catalyst Preparation

The supported catalysts used in this study were prepared by incipient wetness using aqueous solutions of ammonium heptamolybdate $((NH_4)_6Mo_7O_{24} \cdot 4H_2O$ (AHM), Aldrich Chemicals) and/or $(Co(NO_3)_2 \cdot 6H_2O$, Fluka Garantie). When Ni(II) or Fe(III) was impregnated, the nitrate salt of each metal was used and the procedure was the same as the case of supporting Co. The pore volume of the Al_2O_3 support (BET surface area 220 m^2/g) was 0.66 ml/g. This support was a cylindrical extrudate whose diameter was 1/16 in. Three methods were used to prepare Co–Mo/Al_2O_3 catalysts; successive impregnation (first Mo, second

TABLE 1

Nomenclature and Compositions of the Catalyst

Nomenclature:	MoO₃ (wt%)	CoO (wt%)	NiO (wt%)	FeO (wt%)
Successive impregnation (first Mo, second Co)				
M1	1.9			
M2	4.7			
M3	9.7			
M4	14.6			
M5	16.1			
C–M1	1.9	0.4		
C–M2	4.7	1.1		
C–M3	9.5	2.1		
C–M4A	14.4	1.2		
C–M4B	14.1	3.3		
C–M4C	13.6	6.7		
C–M5	15.5	3.8		
N–M5	15.5		3.7	
F–M5	15.5			3.6
Successive impregnation (first Co, second Mo)				
C1		1.0		
C2		3.9		
M–C1	2.3	1.0		
M–C2	15.6	3.3		
Simultaneous impregnation				
CM1	4.4	1.0		
CM2	15.3	3.4		

Co, C–M), successive impregnation (first Co, second Mo, M–C), and simultaneous impregnation (CM). Catalysts, which contained one of the two components, were also prepared. The samples' designation and metal contents are listed in Table 1. After impregnation, these samples were kept at room temperature overnight before drying at 393 K for 12 h. Calcination was conducted in a muffle furnace by ramping at the rate of 10 K/min to 823 K and holding for 4 h, following another hold at 473 K for 1 h. The second impregnation was conducted after calcination when successive impregnation was used. After the second impregnation, a new calcination was done under the same conditions as the first one.

A Co oxide sample was prepared by calcination of cobalt nitrate in air at 823 K for 4 h. A Co–Mo mixed oxide was prepared from the same solution which was used for the preparation of the sample by simultaneous impregnation. After the solution was evaporated at room temperature, it was dried at 393 K overnight and then calcined at 823 K for 4 h.

Titration Procedure

The experimental procedure used for potentiometric titration is described in detail elsewhere (20). A 665 Dosimat (Metrohm) microburette, a thermostated titration vessel,

and a digital Fisher Accumet Model 50 pH meter equipped with a combination glass electrode were used for the measurement. All experiments were conducted under a nitrogen atmosphere at constant temperature (298 K), and constant ionic strength (0.01 N NaNO₃). The solid samples were titrated after equilibration with the inert electrolyte solution (initial volume, V_0). The procedure consisted of adding acid increments (V_a) of titrant and/or base increments (V_b) to the well-agitated suspension and collecting the equilibrium pH data at regular time intervals. The titrant used was either NaOH or HNO₃ solution (volume, V_t) whose normality was 0.1. The proton consumption function was calculated as

$$H_{cons} = V_0(C_a - C_b) + 0.1(V_a - V_b)$$
$$- (V_0 + V_t)\{[H]_f - [OH]_f\}$$

from the analytical concentrations of acid (C_a) and/or base (C_b) and from the actually measured concentrations of H⁺ or OH⁻. The proton consumption function was then normalized with respect to the amount of the titrated sample.

Method of Calculation of the Proton Affinity Distribution (PAD)

If the oxide surface is composed of nonequivalent oxygen groups that differ by their coordinative configuration and acid–base properties, then the heterogeneity may be so complex that a continuous description, rather than discrete one, is needed. The affinity distribution function, $f(pK)$, is defined as the mole fraction of binding sites having the acidity constant in the interval (pK, pK + dpK). For a system of several groups of proton binding sites, the total concentration of deprotonated sites is given by

$$\Theta = \int_{pK_1}^{pK_2} \left[\frac{K}{K + [H]}\right] f(pK)\, dpK,$$

where the bracketed term in the integral takes the form of a Langmuir local isotherm with associated equilibrium constants, K^{-1}. Our approach is to find the distribution function, $f(pK)$, by deconvoluting the experimental proton binding isotherm. We use the approximate method proposed by Rudzinski and Jagiello (RJ) for the calculation of adsorption energy distributions from gas–solid adsorption isotherms (24). The same numerical procedures were used for all samples titrated, including the Al₂O₃ support. A subtle, but important, distinction requires a brief comment; a more expanded discussion can be found in our analysis of the WO₃/Al₂O₃ system (21). For Al₂O₃, the local isotherm is considered to be of the Langmuir form and proton binding/release occurs on surface hydroxyl groups in spe-

cific ranges of pH that can be related to the crystallochemical coordination of OH to aluminium ions in the lattice (19). On the other hand, supported TMOs undergo hydrolysis in specific pH ranges (21), which results in an intense buffering of the solution by the support in that pH window. The buffering intensity is at a maximum for pH values equal to the pK's of particular groups of acidic sites, where inflection points exist on the binding curve. This is equivalent to a change in the proton binding behavior of the solid which is revealed as a peak in the PAD due to the differentiation algorithm which forms the basis of the numerical approximation scheme used. In other words, although the chemistry that underlies the appearance of peaks in PADs for our catalysts is different, the resulting signatures in the PAD are a reliable indication of specific surface structures. All PAD spectra, $f(pK)$, shown in mmol g^{-1} pH^{-1} units in the figures of this paper were arbitrarily shifted along the vertical axis, for clarity. For a quantitative evaluation, the PAD curves were decomposed with Gauss functions and the area under the peaks was evaluated using Peakfit software; peak areas were used for evaluation of the number (mmol g^{-1}) of catalyst surface sites reacting within the corresponding pH range. The estimated accuracy of this approach is $\pm5\%$ when compared to the proton concentration change measured during titration within the corresponding pH range.

Thiophene Hydrodesulfurization

The hydrodesulfurization of thiophene was conducted in a flow system using a microreactor operating at atmospheric pressure. The particle size of the catalyst was 40–80 mesh. Prior to the activity test, each sample of 0.2 g on the basis of oxide was presulfided in a flow of 30 cm³/min of 10% H_2S/H_2 while the temperature was raised to 673 K stepwise and kept at this temperature for 2 h. A gas mixture of 2.46% thiophene (Aldrich Chemical) in H_2 was fed into the U-shaped quartz reactor at the rate of 40 cm³/min. The reaction temperature was raised from 573 to 613 K stepwise and was held at 613 K for 1 h. Thiophene was introduced using a bubbler system and the mole percentage was kept constant in the feed. The concentrations of thiophene in the reactant and the product were analyzed by an on-line gas chromatograph. The thiophene conversion was calculated using these values. The separation of thiophene from hydrocarbons and hydrogen sulfide was conducted under ramping conditions by using a packed column of 23% SP-1720 on 80/100 chromosorb PAW (SUPELCO).

RESULTS

PAD of Mo/Al₂O₃ Samples

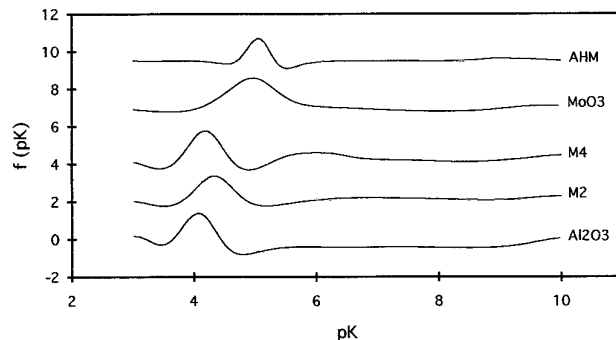Figure 1 shows the PADs for Mo/Al₂O₃ catalysts and references; the latter include the PADs for Al₂O₃, bulk

FIG. 1. Proton affinity distribution of reference Mo compounds (molybdenum oxide, ammonium heptamolybdate), Mo/Al₂O₃ catalysts, and Al₂O₃ support.

MoO₃, as well as the ammonium heptamolybdate salt used to prepare the Mo/Al₂O₃ catalysts. The results show that the supported catalysts have PADs that are significantly different from the bulk oxide. The precursor salt has an affinity spectrum that qualitatively matches that of the unsupported bulk oxide. This is due to the fact that MoO₃ is soluble in water (25), thus its hydrolysis pattern as a function of pH is the same as the dissolved salt. The results shown in Fig. 1 also demonstrate that if any MoO₃ is lost from the support during equilibration, its amount is small or else the PADs of the supported catalysts would have features indicative of the bulk oxide in solution.

PAD of Co/Al₂O₃ Samples

Figure 2 shows the PAD of Al₂O₃, Co/Al₂O₃, and Co oxide as a reference sample. The PAD for the Al₂O₃ used in this study is typical of a gamma Al₂O₃ based on previous data (19, 26). The Co oxide reference has essentially a featureless PAD. This might be the result of its low surface area. Al₂O₃ and Co/Al₂O₃ samples have almost the same signature regardless of the Co content. At low Co content (1 wt%), its strong interaction with the Al₂O₃ support leads
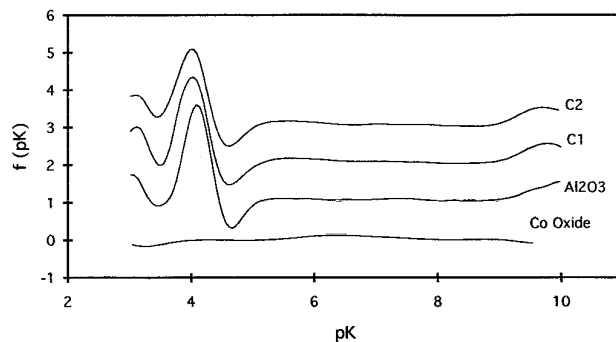

FIG. 2. Proton affinity distribution of reference Co₃O₄, Co/Al₂O₃ catalysts, and Al₂O₃ support.
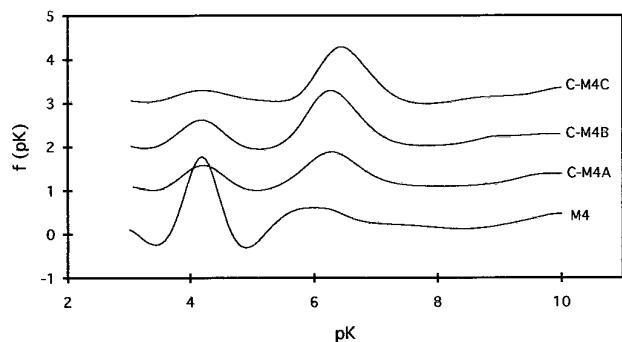
FIG. 3. Proton affinity distribution of Co–Mo/Al$_2$O$_3$ catalysts as a function of Co content. All samples prepared by successive impregnation of Co on the same Mo/Al$_2$O$_3$ (M4). M4:CoO, 0 wt%; C–M4A:CoO, 1.2 wt%; C–M4B:CoO, 3.3 wt%; C–M4C:CoO, 6.7 wt%.

FIG. 4. Proton affinity distribution of Co–Mo/Al$_2$O$_3$ catalysts as a function of Mo content. Both samples prepared by successive impregnation of Co on the Mo/Al$_2$O$_3$ which has different Mo content. C–M2:MoO$_3$, 4.7 wt%; C–M4A:MoO$_3$, 14.4 wt%. The CoO content is fixed at about 1 wt%.

to the formation of a surface CoAl$_2$O$_4$ phase (blue color) which is, structurally, essentially the same spinel type structure as the bare Al$_2$O$_3$ support. The PADs reflect the local structure around hydroxyl groups. Only a small effect of Co on the hydroxyl groups was also shown by Topsøe (27) and by Busca (28) using IR spectroscopy. At higher Co content (3 wt%), Co$_3$O$_4$ is formed (black color) and aggregates on the surface. Thus Co will have little effect on the PAD of the Al$_2$O$_3$ support. The important conclusion is that Co alone on the surface of Al$_2$O$_3$ changes only slightly the PAD of the support and the shape and position of main peaks remain rather similar.

PAD of Co–Mo/Al$_2$O$_3$ Samples

Figure 3 shows the effect of added Co on the PAD of the Mo/Al$_2$O$_3$ (M4) sample whose Mo content is about 14 wt%. The peak centered around pK 6 increases in area as the content of Co increases from 1 wt% (0.90 mmol/g) to 3 wt% (1.23 mmol/g) but the area of the peak does not change for Co loadings over 3 wt% (1.25 mmol/g at 7 wt% Co). We conclude that Co can affect the PAD of Mo/Al$_2$O$_3$ by creating a species whose hydrolysis results in a new peak around pK 6. Because Co has no effect on the PAD of the Al$_2$O$_3$ support (Fig. 2), this peak can not be ascribed to Co-support interaction but can be interpreted as the interaction between Co and the supported Mo. This composition prior to peak saturation corresponds to Co/Mo = 3/7 (molar ratio) and it was reported that Co$_3$O$_4$ is easily formed on the surface of catalysts whose Co/Mo ratio is greater than 0.5 (11). The catalyst containing 7 wt% Co (C-M4C) may have Co$_3$O$_4$ on the surface because the color of this catalyst is black, although the color of the C-M4B is blue.

Figure 4 shows the effect of the content of supported Mo (5 wt% and 15 wt% on an oxide basis) on the PADs of Co–Mo/Al$_2$O$_3$ catalysts. The amount of added Co is fixed at 1 wt%. The PAD signatures differ significantly
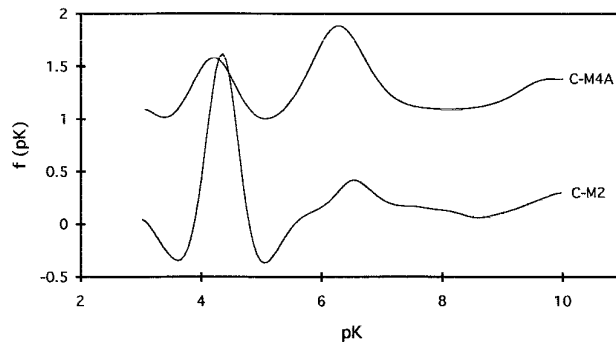
even though the Co content is the same. This result suggests that the nature of the initially supported Mo layer has an influence on the formation of Co–Mo interaction species on the surface of Co–Mo/Al$_2$O$_3$. The higher Mo content catalyst has a pronounced peak centered around pK 6, which we ascribe to Co–Mo interaction species.

Figure 5 further confirms the effect of metal content when Co/Mo ratios are fixed at 3/7 on a molar basis. The peak at pK 6 increases in height with increasing metal content. The peak appears when the Mo content is more than 5 wt% and increases significantly when the Mo content is over 10 wt%.

The effect of preparation procedure of the Co–Mo/Al$_2$O$_3$ catalysts on the PAD signature is shown in Fig. 6. The catalysts have almost the same composition (Co 3 wt% and Mo 14 wt%). The unsupported reference mixed oxide has the same ratio as that in the catalysts. The reference oxide has two main peaks centered around pK 5 and 8. A commercial CoMoO$_4$ also has two main peaks at the same positions as the prepared reference, although the ratio of
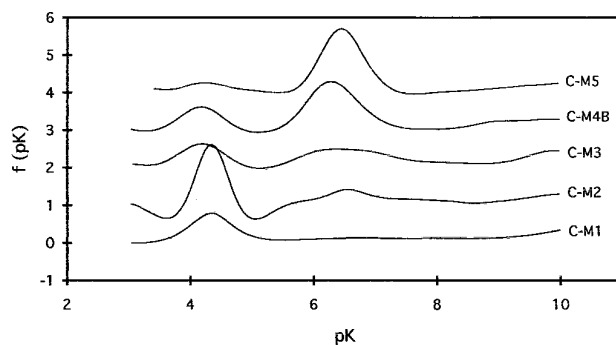

FIG. 5. Proton affinity distribution of Co–Mo/Al$_2$O$_3$ catalysts as a function of total metal content. All samples prepared by successive impregnation. Co/Mo is fixed at 3/7 (atom ratio).
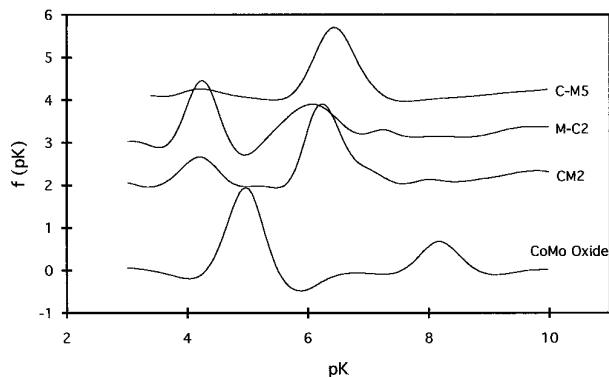
FIG. 6. Proton affinity distribution of high metal content Co/Mo/Al_2O_3 catalysts prepared by different methods: CM2, simultaneous impregnation; M–C2, successive impregnation (first Co, second Mo); C–M5, successive impregnation (first Mo, second Co). The metal contents are fixed. CoMo oxide prepared by drying and calcining of solution of cobalt nitrate and ammonium heptamolybdate.

the two peaks differed. The former peak is at the same pK as the peak of Mo oxide, which might be due to peak overlap with Co–Mo oxide. On the other hand, the latter peak is not in the PAD of either Mo oxide or Co oxide. The latter peak is assigned to a complex oxide which results from calcining the binary solution used for the coimpregnation. The peak, however, is not found in the PADs of the catalysts. The fact that signatures for Co and Mo on the catalysts are quite different from the reference complex oxide points to the existence of the interaction between the supported metal and support and/or the possibility that the two-dimensional chemistry that produces surface complexes is significantly different from the three-dimensional chemistry occurring during bulk metal oxide formation. Figure 6 shows that the peak at around pK 6 of the CM catalyst, which was prepared by simultaneous impregnation, has a similar shape and position when compared to that of the C–M catalyst. The M–C catalyst has a different PAD pattern from the other catalysts and is rather similar to Mo/Al_2O_3 catalyst. This finding is consistent with the fact that Mo adsorption on Co/Al_2O_3 is not affected when Co is present (29) and thus the state of Mo is not remarkably changed whether its support is Al_2O_3 or Co/Al_2O_3. The pertinent finding here is that the peak at pK 6 can be effectively created by either simultaneous impregnation or successive impregnation (first Mo followed by Co).

The results are more subtle as the metal content decreases. Figure 7 shows the effect of the preparation procedure on the PADs for the lower metal content catalysts. On the oxide basis, the Mo content is about 5 wt%, except M–C1, and the Co content is fixed at about 1 wt%. As shown in the figure, the peak around pK 6 is only slightly detected on C-M2 and CM1.
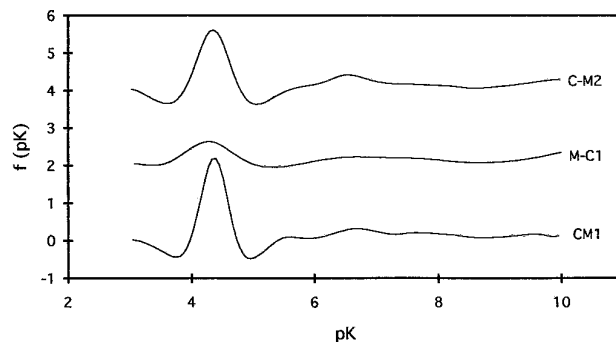

FIG. 7. Proton affinity distribution of low metal content Co/Mo/Al_2O_3 catalysts prepared by different methods: CM1, simultaneous impregnation; M–C1, successive impregnation (first Co, second Mo); C–M2, successive impregnation (first Mo, second Co).

PAD of Ni,Fe–Mo/Al_2O_3 Samples

Figure 8 shows the effect on the PAD when a different second metal is supported on the same Mo/Al_2O_3 (M5). The Ni–Mo/Al_2O_3 catalyst has a PAD similar to that of Co–Mo/Al_2O_3, showing a significant peak around pK 6. On the other hand, Fe–Mo/Al_2O_3 has a different PAD from the other promoted catalysts and the pattern rather resembles that of the original Mo/Al_2O_3. We conclude that the PAD signature is dependent on the element used as the second supported metal.

Thiophene Hydrodesulfurization Activity

Figure 9 shows the relationship between the Co content when the same Mo/Al_2O_3 is used as the support and the thiophene hydrodesulfurization activity. As the Co content increases up to 3 wt%, the activity increases. Over 3 wt%, however, the activity saturates at a value for the conversion of about 58%. The HDS activity is limited at this composition in a manner that parallels the trend of the peak area
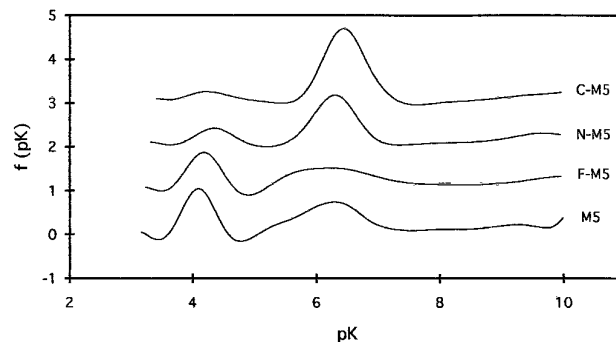

FIG. 8. Proton affinity distribution of promoted Mo/Al_2O_3 catalyst prepared by successive impregnation (first Mo, second promoter). M5, unpromoted Mo/Al_2O_3; F–M5, Fe promoter; N–M5, Ni promoter; C–M5, Co promoter. The metal contents are fixed.
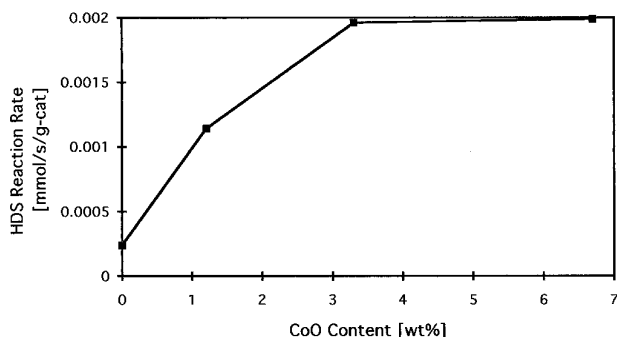
FIG. 9. Thiophene HDS activity as a function of CoO content. All samples prepared by successive impregnation (first Mo, second Co). Reaction conditions: 613 K, 1 atm, 2.46% thiophene in H_2, 0.2 g-cat.

FIG. 11. Effect of promoter on thiophene HDS activity. All samples prepared by successive impregnation (first Mo, second promoter). Reaction conditions: 613 K, 1 atm, 2.46% thiophene in H_2, 0.2 g-cat.

around pK 6 with an increase of the Co content shown in Fig. 2. Taken together these results are consistent with the fact that catalysts show a maximum activity when the composition is promoter/Mo = 3/7 (30).

Two other findings provide additional evidence of the utility of using the signatures of the PADs of this catalyst system to predict their catalytic performance. Figure 10 shows the effect of preparation; the M–C catalyst has a significantly lower activity compared to either C–M or CM catalysts.

Figure 11 shows the effect of the promoter on the HDS activities. The N–M catalyst has an activity similar to that of the C–M catalyst, whereas the F–M catalyst has a much lower activity, close to that of the unpromoted Mo/Al_2O_3 catalyst.

DISCUSSION

The following observations emerge from the affinity distributions for the various catalysts. There appears to be a loading of Mo above which, as more Co promoter is added, a new feature in the PADs appears centered at pK $\sim$ 6.
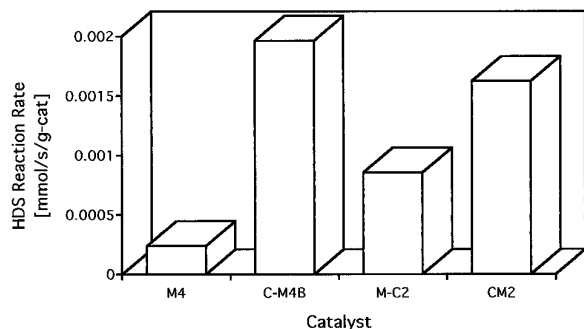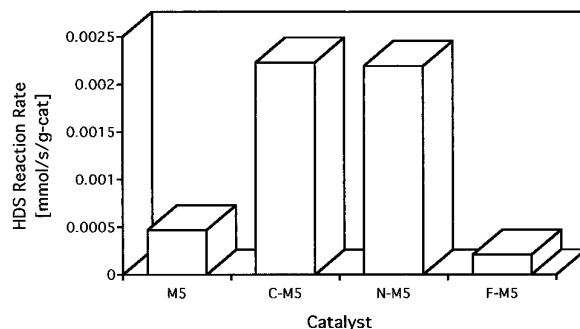

FIG. 10. Effect of preparation method on thiophene HDS activity. The metal contents are fixed. Reaction conditions: 613 K, 1 atm, 2.46% thiophene in H_2, 0.2 g-cat.

As the Co loading is further increased, the area under the feature at pK $\sim$ 6 saturates. Below this Mo loading, the new feature at pK $\sim$ 6 is not as apparent. Simultaneously impregnated catalysts have PADs that are similar to those prepared sequentially (Mo first followed by Co) except the new feature at pK $\sim$ 6 is not as pronounced. If Co is impregnated first, the PADs show no new feature appearing as Mo is added and the affinity distribution is similar to those for Mo/Al_2O_3 catalysts. Finally only certain promoters (Ni) have PADs similar to those when Co is promoter (i.e., Fe).

If we examine the trends in the HDS activities of the catalysts in a manner that parallels the above discussion, the following observations emerge. Above a certain Mo loading, the HDS activity (per gram catalyst basis) increases monotonically with an increase in Co and at a Co/Mo ratio (oxide basis) of $\sim$3/7 the HDS activity saturates. Simultaneously impregnated catalysts show activity trends similar to (but lower than) those of sequentially prepared catalysts (Mo first followed by Co). If Co is impregnated first, catalysts of comparable total oxide loading levels have activities that resemble those if only Mo were present. Ni-promoted catalysts have significantly higher activities than that of Fe promoted catalysts with the latter activities close to those if Mo were present alone.

It is apparent that one common factor links the structure of the catalysts described with their catalytic performance and that is the appearance of a feature in the PADs at pK $\sim$ 6. Recall that features that appear in the affinity distributions of TMOs are the result of hydrolysis of specific surface compounds. The telltale buffering of the electrolyte that occurs in a pH window around 6 indicates that a new surface compound has formed in some of the catalysts studied and that appearance of this structure correlates with the HDS activity of these catalysts.

Recently Deo and Wachs reported on the differences observed in the Raman spectra when dry TMOs are exposed to ambient conditions (23). Their conclusions for
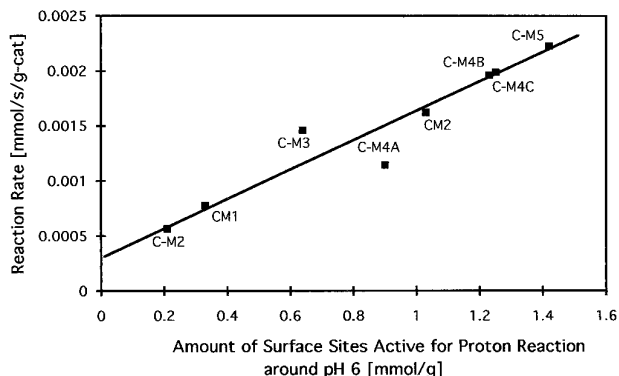
FIG. 12. Relationship between amount of surface sites active for proton reaction around pH 6 and thiophene HDS activity. All samples prepared by successive impregnation (first Mo, second Co) or simultaneous impregnation. Reaction conditions: 613 K, 1 atm, 2.46% thiophene in H_2, 0.2 g-cat.

numerous TMOs are in quantitative agreement with our recent report of the WO_3/Al_2O_3 system and appear to be a general property of these transition metal oxide supported materials when exposed to an environment containing water. Raman spectra of MoO_3/Al_2O_3 indicate the presence of MoO_4^{2-} at low loading and a more complex polyoxyanion ($Mo_7O_{24}^{6-}$) at higher loading. Furthermore they also concluded that the presence of promoters can alter the surface metal oxide structures under ambient (aquated) conditions. Changes in the structure of the TMOs at various loadings were shown to be consistent with pH values that reflect the speciation of the salt used to prepare the TMO supported catalysts under homogeneous conditions.

It is important to note at this point our observed affinity distribution, at a fixed weight loading, provide a complete delineation of all structures hydrolyzed over the pH range used during the potentiometric titration; structures actually present are determined by the prevailing conditions which include metal loading and pH during promotor addition.

To examine further the hypothesis that the structure responsible for the feature at pK $\sim$ 6 seen in the PADs can be correlated with the HDS activity, we present in Fig. 12 the activity data recorded under standard conditions for the catalysts studied as a function of the area under the pK $\sim$ 6 feature. The latter quantity, on the basis of the working hypothesis, is proportional to the number of active catalytic sites. The points are CM and C–M catalysts of various metal loading and the line is the best fit to the data. As shown in this figure, the increase in the HDS activity is proportional to the number of these sites before sulfiding. The observation that the line in this figure does not pass through the origin is a consequence of the fact that the unpromoted catalysts have some activity. Wivel et al. reported a similar linear relationship between HDS activity and absolute amount of octahedral Co in Co/Mo/ Al_2O_3 catalysts in the oxide state (11). They concluded

that the surface species, octahedral Co, are the precursor for the active sites. Although it is not only the octahedral Co in the oxidic precursor that might end up as Co in "Co–Mo–S" in the activated catalyst (14), we assume that the feature at pK $\sim$ 6 could be due to a structure containing mainly octahedral Co.

Johnson et al. studied the structure of a series of Co/ Mo/Al_2O_3 catalysts in their oxidized state by EXAFS (31). They found that an increase in the Mo loading was accompanied by a decrease in the apparent coordination number about the molybdenum which was an indication of major distortions of the MoO_6 octahedra. The addition of Co to the Mo/Al_2O_3 catalysts led to a decrease in distortion but this became most apparent only when the Mo loading was greater than $\sim$6%. While it is not directly apparent what the relationship between the EXAFS results have in common with the evaluation in PADs of Co/Mo/Al_2O_3 catalysts of this study, there is a parallelism which leads us to speculate further.

From these results, it is proposed that Co in Co/Mo/ Al_2O_3 catalysts is octahedral and Co is neighboring MoO_6 octahedra and interacts directly with it. It is further proposed that this surface Co–Mo interaction species might have a heteropolymolybdate-like structure in the oxide state and that the feature at pK $\sim$ 6 observed in this study might be the hydrolysis of such a species. Spojakina et al. also suggested the possibility of nickel heteromolybdate existing on the oxide catalyst (32). As mentioned earlier, a continuation of this study provides XPS, Raman, and TPR results which are consistent with the above speculation (33).

Two other findings reported herein require some discussion. The coimpregnated catalyst has an activity (and PAD at pK $\sim$ 6) that is lower than C–M catalysts of comparable composition (but higher than the unpromoted catalyst). Recently, Spanos and Lycourghiotis (34) reported that there was a synergistic effect on Co^{2+} adsorption on Al_2O_3 in the presence of Mo. This could be rationalized on the basis of a strong affinity of the counterions in the aqueous phase prior to their deposition on the support. If Co and Mo have associated into a complex and it survives drying and calcination steps, then structures similar to, but less well-defined, than those discussed above could result. To speculate on this issue further is not warranted.

Finally, why does iron not show the same promoting effects as Ni or Co? The singular difference in the preparation of the Fe-promoted catalysts was that Fe(III) was the precursor. The aqueous phase chemistry of Fe(III) is considerably more complex than that of Fe(II) (or Ni(II) and Co(II)) (35). Formation of dinuclear species $Fe_2(OH)_2^{4+}$ in acidic solutions (conditions existing during Fe(III) addition) might compete with the possible formation of heteropoly-compounds. Then we would expect the

activity (and PADs) to be more similar to the unpromoted catalysts, which they were. Another explanation offered by Ramselaar *et al.* (36) was that the promoting effect of Fe depends strongly on the sulfiding procedure. However, our results show that at least for this set of catalysts, the difference between the Fe-promoted catalyst and the Co- or Ni-promoted catalysts appeared even in the oxidic phase.

CONCLUSIONS

From the discussions above, this study can be summarized as follows: (1) A Co–Mo interaction species can be identified in the oxide state by using PADs. (2) The amount is proportional to the thiophene hydrodesulfurization activity after sulfiding. (3) Successively impregnated Mo–Co (first Co, second Mo) can create the Co–Mo interaction species but not as effectively as successively impregnated Co–Mo (first Mo, second Co) or simultaneously impregnated CoMo. (4) Ni(II) also interacts with Mo and can be used as a promotor whereas Fe(III) cannot.

ACKNOWLEDGMENT

REFERENCES

1. Topsøe, H., Clausen, B. S. Candia, R., Wivel, C., and Mørup, S., *J. Catal.* **68,** 433 (1981).
2. Wivel, C., Candia, R., Clausen, B. S., Mørup, S., and Topsøe, H., *J. Catal.* **68,** 453 (1981).
3. Louwers, S. P. A., and Prins, R., *J. Catal.* **133,** 94 (1992).
4. Upton, B. H., Chen, C. C., Rodriguez, N. M., and Baker, R. T. K., *J. Catal.* **141,** 171 (1993).
5. Kabe, T., Qian, W., and Ishihara, A., *J. Catal.* **149,** 171 (1994).
6. Crajé, M. W. J., deBeer, V. H. J., van Veen, J. A. R., and van der Kraan, A. M., *Appl. Catal.* **100,** 97 (1993).
7. Crajé, M. W. J., deBeer, V. H. J., van Veen, J. A. R., and van der Kraan, A. M., *J. Catal.* **143,** 601 (1993).
8. Crajé, M. W. J., deBeer, V. H. J., van Veen, J. A. R., and van der Kraan, A. M., *in* "Symposium of Advances in Hydrotreating Catalysts, ACS Meeting, Washington, DC, August 21–26, 1994."
9. Topsøe, N., and Topsøe, H., *J. Catal.* **75,** 354 (1982).
10. Kasztelan, S., Grimblot, J., and Bonnelle, J. P., *J. Phys. Chem.* **91,** 1503 (1987).
11. Wivel, C., Clausen, B. S., Candia, R., Mørup, S., and Topsøe, H., *J. Catal.* **87,** 497 (1984).
12. Clausen, B. S., Topsøe, H., Candia, R., and Villadsen, J., *J. Phys. Chem.* **85,** 3868 (1981).
13. Clausen, B. S., Lengeler, B., and Topsøe, H., *Polyhedron* **5,** 199 (1986).
14. van Veen, J. A. R., Gerkema, E., van der Kraan, A. M., Hendriks, P. A. J. M., and Beens, H., *J. Catal.* **133,** 112 (1992).
15. Kasztelan, S., Payen, E., Toulhoat, H., Grimblot, J., and Bonnelle, J. P., *Polyhedron* **5,** 157 (1986).
16. Dufresne, P., Payen, E., Grimblot, J., and Bonnelle, J. P., *J. Phys. Chem.* **85,** 2344 (1981).
17. Zhang, R., Schwarz, J. A., Dayte, A., and Baltrus, J. P., *J. Catal.* **135,** 200 (1992).
18. Southmayd, D. W., Contescu, Cr. Schwarz, J. A., *J. Chem. Soc. Faraday Trans.* **89,** 2075 (1993).
19. Contescu, Cr., Jagiello, J., and Schwarz, J. A., *Langmuir* **9,** 1754 (1993).
20. Schwarz, J. A., Contescu, Cr., and Jagiello, J., "Catalysis," Vol. 11, p. 127, Specialist Periodical Report, Royal Society of Chemistry. Cambridge, Thomas Graham House, 1994.
21. Contescu, Cr., Jagiello, J., and Schwarz, J. A., *J. Phys. Chem.* **97,** 10152 (1993).
22. Contescu, Cr., Popa, V. T., Miller, J. B., Ko, E. I., and Schwarz, J. A., *J. Catal.,* **157,** 244 (1995).
23. Deo, G., and Wachs, I. E., *J. Phys. Chem.* **95,** 5889 (1991).
24. Rudzinski, W., Jagiello, J., and Grillet, Y., *J. Colloid Interface Sci.* **87,** 478 (1982).
25. "Handbook of Chemistry and Physics," 53rd ed., p. B-111. Cleveland, The Chemical Rubber Co., 1972.
26. Contescu, Cr., and Schwarz, J. A., *Appl. Catal.* **118,** L5 (1994).
27. Topsøe, N., *J. Catal.* **64,** 235 (1980).
28. Busca, G., Lorenzelli, V., Escribano, V. S., and Guidetti, R., *J. Catal.* **131,** 167 (1991).
29. Siri, G. J., Morales, M. I., Blanco, M. N., and Thomas, H. J., *Appl. Catal.* **19,** 49 (1985).
30. Ahuja, S. P., Derrien, M. L., and Le Page, J. F., *Ind. Eng. Chem. Prod. Res. Develop.* **9,** 272 (1970).
31. Chiu, N. S., Bauer, S. H., Johnson, M. F. L., *J. Catal.* **89,** 226 (1984).
32. Spojakina, A., Damyanova, S., Petrov, L., and Vit, Z., *Appl. Catal.* **56,** 163 (1989).
33. Adachi, M., Contescu, Cr., and Schwarz, J. A., in preparation.
34. Spanos, N. and Lycourghiotis, A., *Langmuir* **10,** 2351 (1994).
35. Baes, C. F. and Mesmer, R. E., "The Hydrolysis of Cations," p. 237. New York, 1976.
36. Ramselaar, W. L. T. M., Crajé, M. W. J., Gerkema, E., de Beer, V. H. J., and van der Kraan, A. M., *Bull. Soc. Chim. Belg.* **96**, 931 (1987).